

# Chapter 5

## Estimation of pore pressure variation induced reflectivity pattern changes at the KTB test site.

### 5.1 Geological settings

After more than a decade of geoscientific research at the German Continental Deep Drilling Site (KTB) a new large interdisciplinary research project has been initiated in order to exploit the geoscientific potential of this unique test site. This frame project is called *Energy and Fluid Transport in Continental Fault Systems*. Within the center of many involved projects a series of pumping and injection test within the SE1 and SE2 fault zones (see Fig. 5.1 and 5.3) and the monitoring of thereby induced chemical and physical processes is planned.

One branch of monitoring experiments is 4D reflection seismics. Field examples of such experiments and rock physical laboratory investigations from the hydrocarbon industry show, that pumping and injection of fluids might cause significant variations of the subsurface reflection pattern over time. The aim of such experiments is to extract information about in-situ stress, fluid pressure, hydrocarbon flow paths, fluid saturation changes, fluid properties and so on from reflectivity pattern changes.

In this context, one key issue of the DFG project *4D modelling of seismic signature of fluid flow in crystalline rocks* is presented. This project was designed to obtain an estimation of the magnitude of possible reflectivity pattern changes along the SE2-host rock interface due to artificially induced pore pressure variations, e.g., by pumping and injection test.

The geology of the KTB site was investigated by numerous scientists over the last years. Detailed descriptions can be found in, e.g., Wagner *et al.* (1997); O'Brien *et al.* (1997). Here, only a brief geological overview is given. A more detailed summary will only be given for topics, which are important for this study.

The drill site of the *German Continental Deep Drilling Program* (KTB) is located

## 5.1. Geological settings

in the Zone of Erbdorf-Vohenstrauss (ZEV) at the western border of the Bohemian massive. This small, isolated tectonometamorphic unit, which is characterized by an association of paragneisses, amphibolites, orthogneisses, and metapegmatites is located close to the boundary of three major crustal units, the Saxothuringicum, the Moldanubicum, and the Bohemian Block. These large geological units were formed during the Variscian orogeny as a result of the collision between Laurasia and Gondwana and intervening microcontinents and oceanic fragments. A major NW-SE trending fault zone, the Frankonian Lineament, separates these crystalline rocks from Permo-Mesozoic cover in the west. In the north, east, and south it is delimited by a low-pressure metamorphic imbrication zone (O'Brien *et al.*, 1997). Figure 5.1 shows a three dimensional interpretation of the local geology.

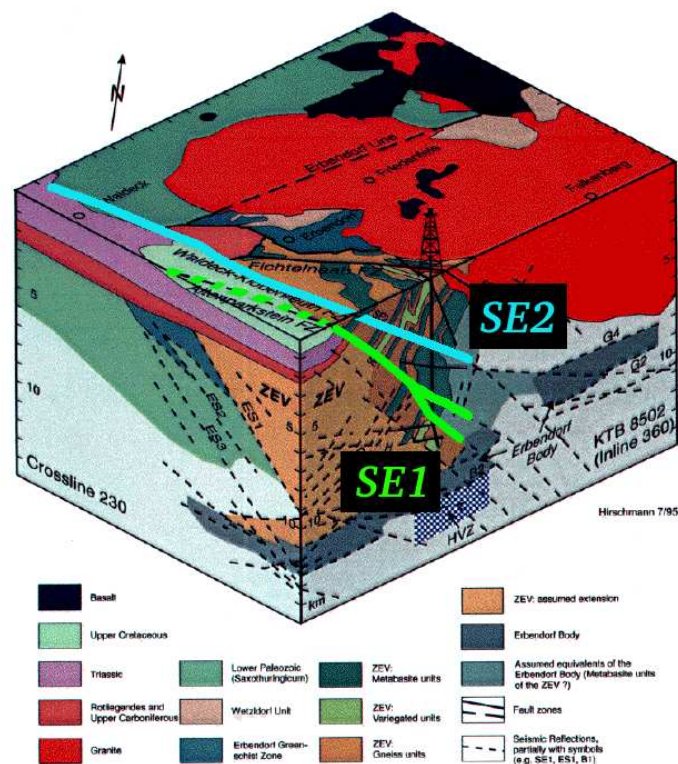


Figure 5.1: 3D geological interpretation of the KTB test site. The SE1 and SE2 fault zones are indicated as green and light blue lines, respectively. Picture taken from Harjes *et al.* (1997), slightly modified.

The drilled crustal section can be subdivided into three major lithological units: (1) Paragneisses derived from turbiditic greywackes, (2) massive metabasitic units of igneous origin with enriched mid-ocean ridge basalt characteristic, and (3) varied units of partly calc-silicate bearing paragneis-metabasites alterations of former vulcanosedimentary sequences (Pechnig *et al.*, 1997). In the KTB main hole (KTB-HB) unit 1 reaches from 0 to 3200 m, unit 2 from 3200 to approx. 7300 m and unit 3 can be found between 290-552 m, 2384-2718 m and 7260-7800 m. From 7800 m to the final depth of 9101 m paragneisses dominate with an increasing amount of amphibolite intercalations below 8080 m. The KTB pilot hole (KTB-VB) was drilled over almost its entire length down to 3575 m through Unit 1. Below that depth unit 2 was drilled and from 0-560 m and from 2470 to 2690 m unit 3 (Berckhemer *et al.*, 1997).

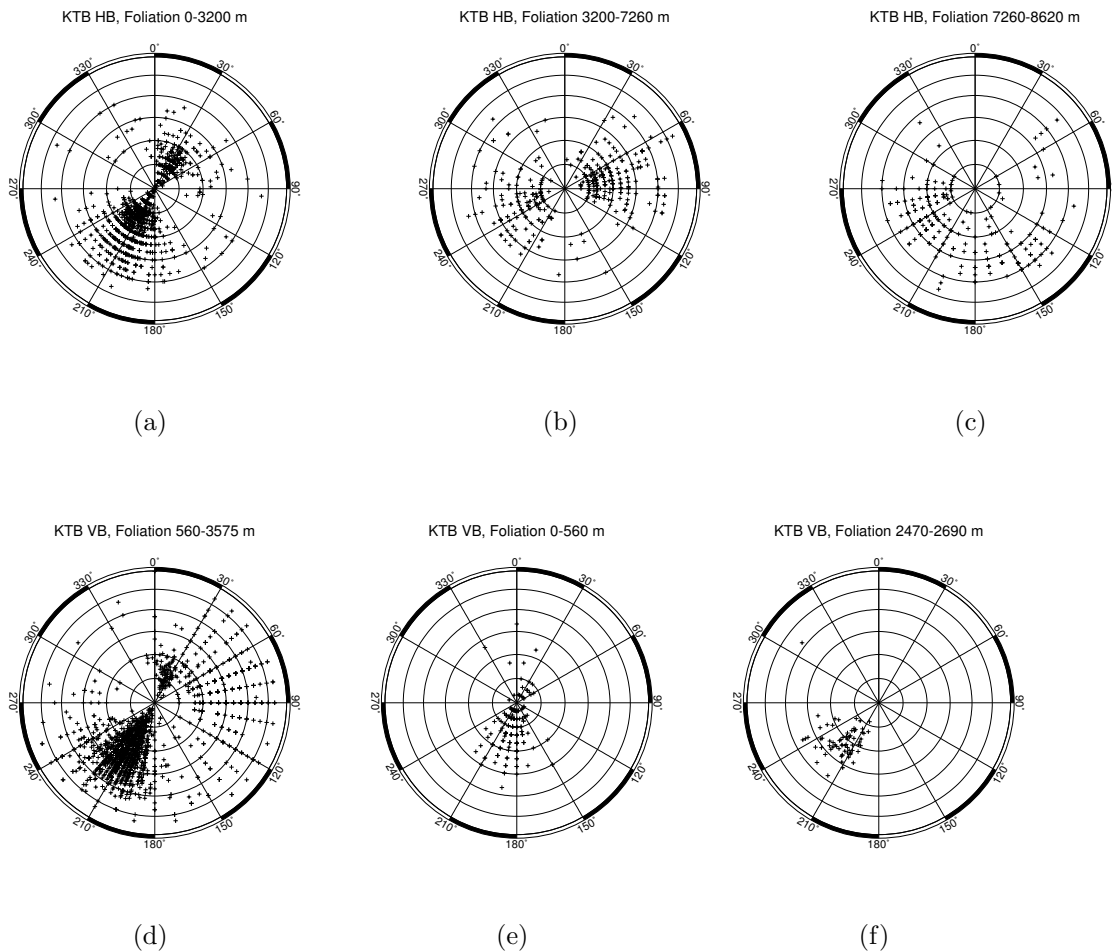


Figure 5.2: Dip of foliation in the KTB-HB, figures 5.2(a) - 5.2(c) and KTB-VB, figures 5.2(d) - 5.2(f), in Lambert projection. Based on the distribution of dip azimuth Berckhemer *et al.* (1997) subdivided the HB rocks into three structural units: unit 1 (Fig. 5.2(a) and 5.2(d)), unit 2 (Fig. 5.2(b) and 5.2(e)), and unit 3 (Fig. 5.2(c) and 5.2(f)). Data from <http://icdp.gfz-potsdam.de/html/ktb/ktb.htm>.

Paragneisses and hornblende gneisses show an intensive foliation and a NNW-SSE oriented, subhorizontal stretching lineation. In contrast, the metabasites are deformed more inhomogeneously; undeformed metagabbros with preserved magmatic textures are often located close to foliated amphibolites (O'Brien *et al.*, 1997). According to Berckhemer *et al.* (1997), foliation in general dips steeply to the SW or NE with angles between 60 and 80°. Foliation occurs in large-scale folds with subhorizontal axial planes and fold axis trending to NNW-SSE. Dip direction of the foliation allows for subdividing the KTB-HB into three structural units: unit 1 from 0-3200 m, unit 2 from 3200-7260 m and unit 3 from 7269-8620 m. Foliation in unit 1 dips mainly to SW and minor to NE, mainly to east and minor to west in unit 2, and to SW in unit 3, as shown in figure 5.2.

The distribution of dip direction of the foliation in the KTB-VB cannot be used to subdivide the drilled rocks structurally, since the KTB-VB drilled almost entirely through lithological unit 2 and the number of measurements in unit 1 and 3 do not allow a significant statement about the preferred dip azimuth.

## 5.1. Geological settings

Both boreholes cut numerous cataclastic fracture zones. The most extensive fault zone is crossed by the KTB-HB between 6850 and 7260 m and is characterized by a high percentage of cataclastic rocks and strong alteration. It strikes with  $140^\circ$  from north and dips  $55^\circ$  to  $60^\circ$  to NE. It correlates with the surface trace of the Frankonian Lineament which is mapped approx. 5 km SW of the drilling site (Berckhemer *et al.*, 1997). This fracture zone is associated with the most prominent seismic reflector, the seismic event SE1, which cuts the upper crust down to a depth of approx. 10 km. In a depth range of approx. 3800 to 4000 m both bore holes penetrate the seismic event SE2 (Fig. 5.3).

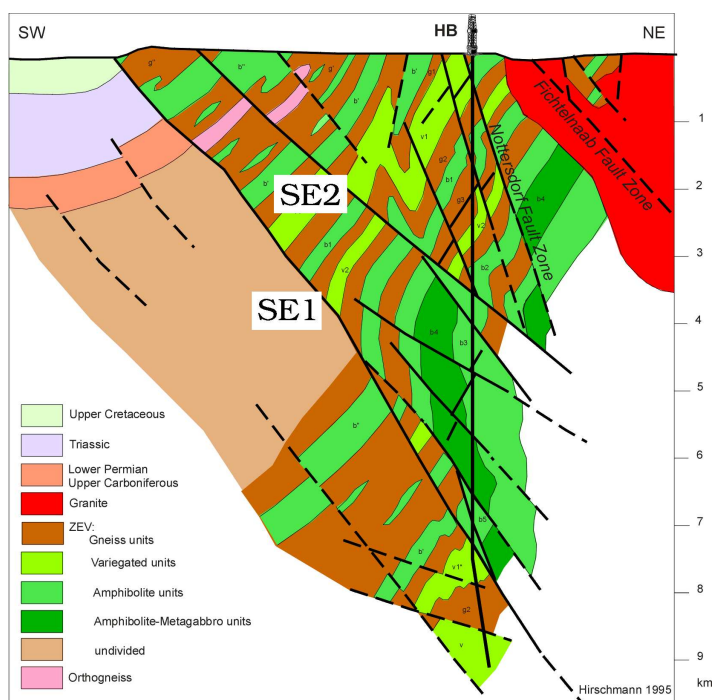


Figure 5.3: SW-NE cross section through the KTB test site. From Emmermann & Lauterjung (1997), slightly modified.

The KTB boreholes enable a detailed investigation of the petrophysical properties of the continental crystalline crust down to a depth of 9101 m. Of special interest is the comparison of surface measurement, borehole log, and laboratory derived results. Whereas the KTB-VB was cored almost completely down to 3880 m and data are available from sampling intervals less than 2 m, the petrophysical investigation of the KTB-HB rocks is mainly based on the analysis of drill cuttings. Coring in the KTB-HB started below 4150 m but is limited to a total recovery of not more than 83.6 m (Berckhemer *et al.*, 1997).

### 5.1.1 Steep elements SE1 and SE2 as seismic reflectors

The SE1 and SE2 reflectors are the main targets of the coming seismo-hydraulic experiments. The latter is penetrated by the KTB-VB and the KTB-HB in a depth

of approx. 4 km. The deeper SE1 is only crossed by the KTB-HB in a depth interval between approx. 6850 and 7300 m. Until now, it is still an open question which drilled fault or faults within that section represent the seismic reflection.

From a former 2-D survey (denoted as KTB8502), which was oriented approx. perpendicular to the strike of the SE1 it is known that the SE1 penetrates the whole upper crust down to more than 10 km depth. It separates perme-mesozoic foreland sediments in the southwest with P-wave velocities of 3-4 km/s from crystalline basement rocks in its northeast with P-wave velocities of 5-6 km/s. Based on a 2-D prestack Kirchhoff migrated image of the KTB8502 line the dip of the SE1 can be estimated as about 55 degrees (Buske, 1999).

Figure (5.4) shows selected slices from a 3-D prestack Kirchhoff migration of the ISO89-3D seismic data set (Buske, 1999). The migrated volume covers an area of 21x21 km<sup>2</sup> centered around the KTB and reaches 15 km depth. A general result of this study is that the SE1 is a clear seismic reflector over its entire depth but with a complex structure and regions where the reflection is sharp and regions where the reflection becomes more diffusive. Unfortunately, the KTB-HB crosses the SE1 at such a diffusive region. This corresponds to borehole results where the SE1 appears as a cataclastic zone of several hundred meter thickness. At the top of this zone (6860 m) sonic P-wave velocity drops from an average value of 6.5-6.2 km/s with significant variations. Together with even larger density variations, impedance fluctuations reach 20-30% which correspond to reflection coefficients between 0.1 and 0.15. The S-wave velocity drops by about 5% to 3.4 km/s (Harjes *et al.*, 1997).

## 5.2 Seismic anisotropy

From different investigations it is known that the petrophysical properties of most KTB rocks show a significant anisotropy (e.g., Berckhemer *et al.*, 1997). Laboratory measurements on cores under normal conditions reveal ranges from a few percent for P-wave velocity and up to 80% for P-wave amplitudes. These measurements were conducted on planes perpendicular to the drill core axis. However, an example from the KTB-HB from 5282 m (foliated hornblende gneiss) shows that the direction of the long axis coincides for all properties under consideration with the strike of the foliation. Microcracks are preferably aligned in the direction of foliation (Zinke, 1996; Siegesmund *et al.*, 1993a,b). According to Kern *et al.* (1991, 1994), the seismically effective cracks are oriented parallel to the foliation and thus normal to the present minimum principal stress axis  $\sigma_h$  (Brudy *et al.*, 1997). A sufficient agreement between measured P-wave velocity anisotropy (under normal conditions) and calculated values derived from crack density distribution velocities using Hudson's theory (Hudson, 1981) indicates strongly that the velocity anisotropy is largely affected by microcracks. Especially attenuation turned out to be highly sensitive to the preferred orientation of microcracks with its maximum perpendicular to the cracks. Laboratory measurements of velocity anisotropy under increasing confining pressure are a tool to distinguish between fabric and crack induced anisotropy. Berckhemer *et al.* (1997) infer from such tests that anisotropy is dominated by cracks in the low-confining pressure regime. With increasing confining pressure anisotropy decreases and tends towards a more or less stable value. This stable level is reached above 200 MPa where almost all cracks are assumed to be closed. The

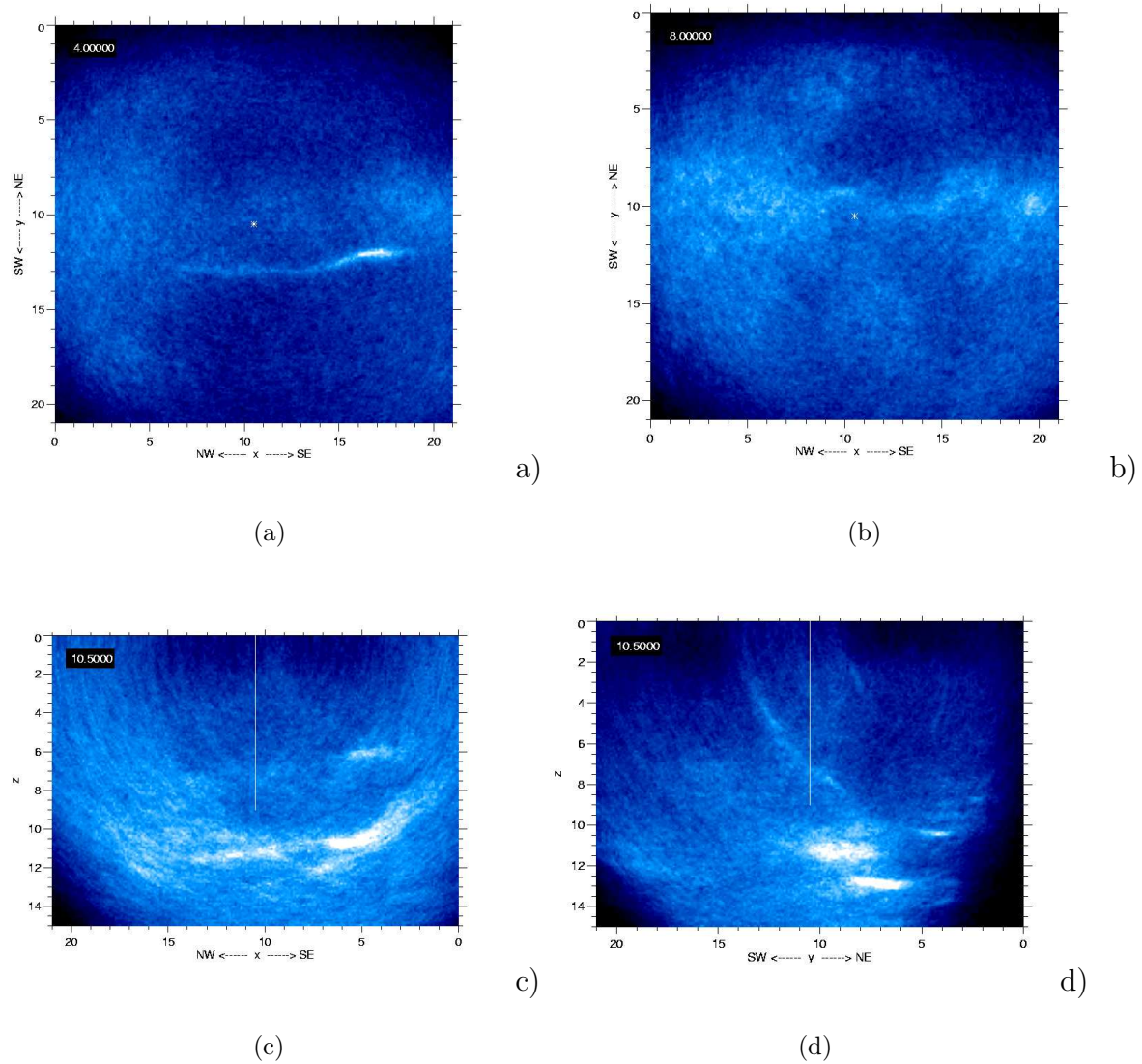


Figure 5.4: Selected slices of 3-D prestack Kirchhoff migration of the ISO89-3D data set (Buske, 1999). The slices belong to a  $21 \times 21 \times 15$  km data volume centered around the KTB. Fig. 5.4(a) and 5.4(b) show horizontal slices through the volume in 4 km and 8 km depth, respectively. The grey cross in the middle of both plots indicates the position of the KTB. Fig. 5.4(c): Vertical slice normal to the  $y$ -axis at  $y=10.5$  km. The slice is oriented approx. parallel to the strike of the SE1. Fig. 5.4(d): Vertical slice normal to the  $x$ -axis of the volume and normal to the strike of the SE1 at  $y=10.5$  km. In both latter plots, the KTB is located at horizontal position 10.5 km.

residual anisotropy is interpreted to be caused by the preferred orientation of minerals. Gneisses show the highest residual anisotropy which is addressed to the alignment of phyllosilicates.

The analysis of S-wave anisotropy, also called *shear wave splitting* (SWS), is the most important tool for characterizing anisotropic elastic media. SWS is characteristic for the anisotropic KTB gneisses. It is strongly related to the foliation and most dominant for propagation parallel to the foliation. The fast S-wave is polarized parallel, the slow S-wave normal to the foliation (Berckhemer *et al.*, 1997).

A comparison of VSP data with laboratory data from 13 samples (depth range 2000-3000 m) shows strong differences both in P-wave velocity and anisotropy, whereas S-wave velocity and anisotropy are in a good agreement. This indicates that upscaling of laboratory derived seismic velocities to in situ velocities is not straightforward.

Bokelmann & Harjes (2000) document a systematic temporal variation of the seismic anisotropy due to the 1994 injection test at 9101 m. During the experiment the difference between shear wave velocities decreased by approx. 2 % within 12 h. They explain this phenomenon by stress release due to the induced microseismicity. The seismic events decrease the state of stress in a way, that  $\sigma_1$  decreases but  $\sigma_3$  increases. As a result all fractures aligned normal to  $\sigma_3$  should close and thus shear wave splitting should decrease.

### 5.3 KTB fluids

One of the main goals of the proposed hydraulic tests at the KTB is to pump uncontaminated fluids, which has not been possible, yet. Most of the chemical and isotopical results from sample analysis are contaminated by drilling mud additives.

In the KTB-VB a short-term pumping test was performed in the open hole section at 3850-4000m. About 71  $m^3$  of Ca-Na-Cl fluids and accompanying gas, containing mainly  $N_2$  and  $CH_4$ , were pumped (Möller *et al.*, 1997). To overcome the contamination a second pumping test lasting several months was performed from August to December 1991. Table 5.1 shows the chemical composition of the KTB fluids developed in the KTB pilot hole at 4000 m depth.

The main components Ca, Na, and Cl represent 97.6% and 98.1% of the total dissolved solids for the April 1990 and December 1991 sample, respectively. As shown in Fig. (5.5) the three major components dominate the chemical composition clearly.

In the KTB-VB groundwater occurs down to a depth of at least 650 m (Möller *et al.*, 1997). Below 3400 m several fractures containing high-saline fluids were detected. According to Kessels (1991) and Lodemann *et al.* (1997), all fractures act as isolated systems with the exception of the main fracture system near the bottom of the KTB-VB (SE2) as indicated by hydraulic data.

The results of the chemical analysis of the pumped brine can be summarized in that way, that (1) fluid salinity increases with depth, and (2) the composition changes from Na- dominated to Ca-dominated at the bottom of the KTB-VB (Huenges *et al.*, 1997). In situ temperature was 119° C, fluid pressure was 40 MPa.

### 5.3. KTB fluids

Table 5.1: Main composition of KTB fluids pumped from VB at 4000m (from Möller *et al.* (1997) after Pekdeger *et al.* (1994) and Lodemann *et al.* (1997)).

Contents mg/l	Samples	
	April 12, 1990	Dec. 17, 1991
$Na^+$	5500	7159
$Ca^{2+}$	14700	15700
$K^+$	200	231
$Mg^{2+}$	6.8	2.19
$Sr^{2+}$	270	244
$Li^+$	5.4	2.41
$Al^{3+}$	0.07	<0.013
$SiO_2$	50.7	54
$Cl^-$	39500	44100
$Br^-$	493	417
$F$	1.45	3.82
$SO_4^{2-}$	390	307
$HCO_3^-$	97.6	45.1
DOC	50.2	1.2-5.4
TDS	61170	68260

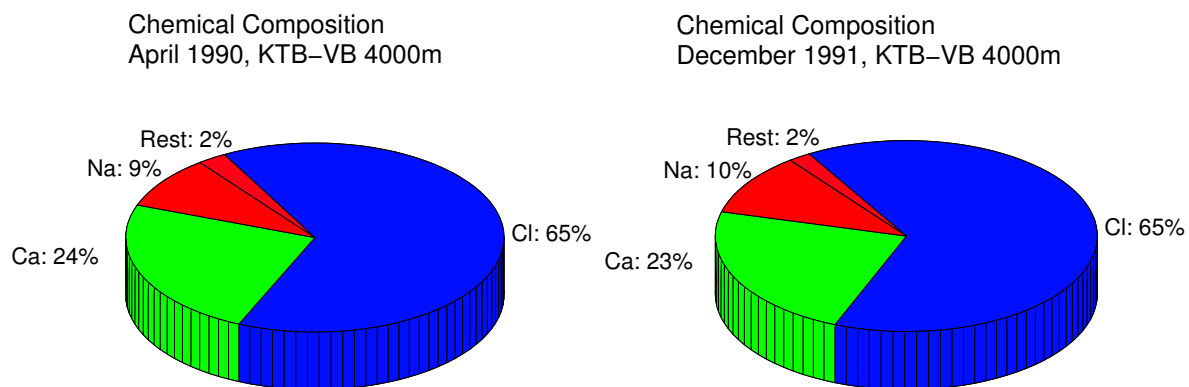


Figure 5.5: Chemical composition of KTB-VB fracture water from pumping tests in April 1990 (left) and December 1991 (right) in 4000 m depth.

In addition to the chemical composition of brine the composition of the gas phase released from the brine was monitored. The gas phase is dominated by  $N_2$  and  $CH_4$  (Möller *et al.*, 1997). A similar composition was monitored in the KTB-HB between 3063 and 6031 m (Engeser *et al.*, 1993). Modeling the seismic signature of the KTB fluids requires the determination of the fluids bulk modulus  $K_{fl}$  and its density  $\rho_{fl}$  as a function of pressure  $P_{fl}$ , temperature  $T$ , and salinity  $c$  of sodium chloride (NaCl). Therefore, we use the empirical relations from Batzle & Wang (1992). The relation between the fluid bulk modulus  $K_{fl}$  and the acoustic velocity  $v_a$  is  $K_{fl} = \rho_{fl} \cdot v_a^2$ .

The mean pore pressure gradient down to 9101 m was determined to 11.5 MPa/km. It increases over a transition zone between 2000 m and 3400 m from 9.8 to 10.5 MPa/km due to an increase in density from 1000 to 1060  $g/cm^3$ . Between 6000 m and bottom hole the gradient increases again (Huenges *et al.*, 1997). With a bottom hole pore pressure of 103 MPa the gradient below 6000 m increases again.

Assuming hydrostatic pore pressure conditions down to 9101 m requires a remarkable fluid density increase below 6000 m depth which could be explained by an increasing salinity. At 4000 m depth the NaCl content is 68 g/l which could correspond to 1 mol NaCl. Analysis of samples in the KTB-HB between 4000 and 5400 m show a higher salinity with about 1.5 mol NaCl equivalent. Unfortunately, downhole sampling was not successful below 5500 m. An extrapolation of the NaCl salinity which is required for using Batzle and Wang's relation in order to calculate the depth dependence of the fluid bulk modulus is further complicated by a change from Na to Ca domination. However, we assumed a NaCl salinity at the surface of 500 mg/l and interpolated the NaCl content with the measured values at 4000 m depth down to 9101 m linearly. Therefore we have to emphasize, that this is critical below 4000 m. The temperature profile was calculated linearly with a gradient of 28° C/km. Finally, the depth dependence of the mentioned properties of the KTB fluid as used for the calculation of the fluid bulk modulus is shown in Fig. (5.6).

Figure (5.6(d)) shows the final estimation of fluid bulk modulus profile. The blue circles show the result for a density profile as calculated from the pressure profile and the green line results from using a calculated density according to Batzle & Wang (1992) as a function of salinity, temperature, and pressure. Both curves are in good agreement down to 4000 m with a mean bulk modulus of 2.1 to 2.9 GPa. The strong deviation between both curves indicate, that a calculation of  $K_{fl}$  below 4000 m is very critical.

## 5.4 Rock physical properties

### 5.4.1 Porosity of the KTB rocks

The KTB rocks show two different porosity and permeability domains. The rock matrix dominates the magnitude of the bulk porosity of the system but shows a low permeability, whereas the fracture system has a very low porosity but controls the permeability. Therefore, the KTB rocks can be characterized as a double-porosity system (Möller *et al.*, 1997).

## 5.4. Rock physical properties

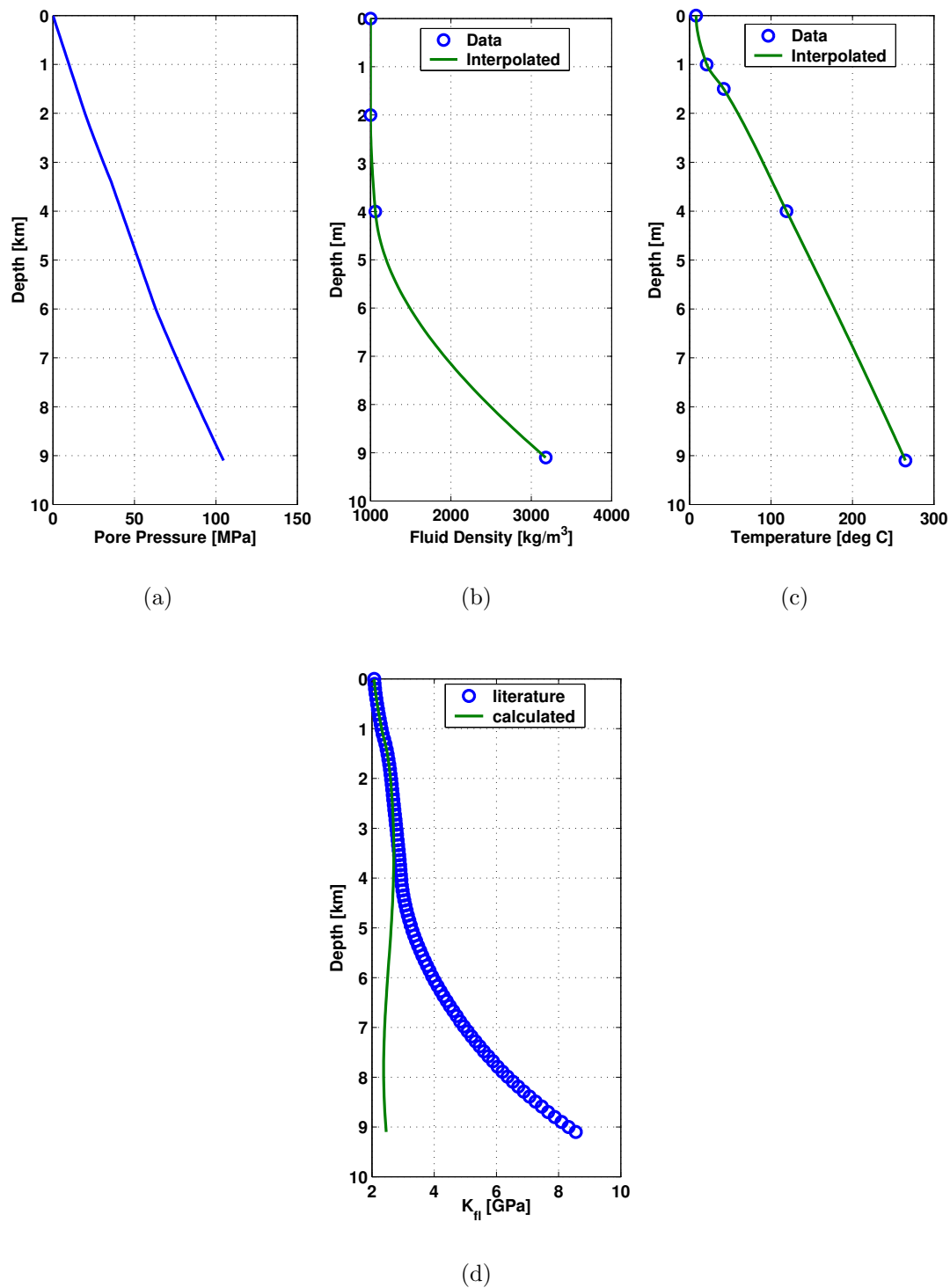


Figure 5.6: Depth dependence of KTB fluid properties according to Huenges *et al.* (1997). Fig. 5.6(a) to 5.6(c) show pore pressure, fluid density, and temperature, respectively. Fig. 5.6(d): The resulting depth depending bulk modulus of the fluid was calculated according to Batzle & Wang (1992).

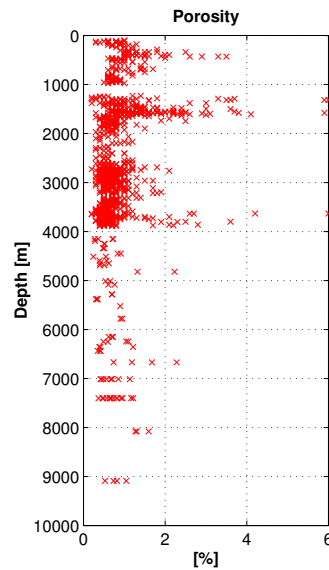


Figure 5.7: Porosity profile down to 9101 m. Zones of enhanced porosity are interpreted as regions where fault zones cross the bore holes.

Laboratory measurements on relaxed plug samples from both boreholes yielded a porosity of  $1\% \pm 0.4\%$  (Huenges *et al.*, 1997). Figure (5.7) illustrates the porosity profile down to 9101 m. The porosity was determined using the Archimedian method which also allows for estimating the density of the rock matrix <sup>1</sup>. The profile illustrates the mean porosity as mentioned above but shows clear deviations towards maximum values between 4 and 6% where fault systems are crossed by the boreholes. The dense sampling at the KTB-VB allows to identify three clear zones of enhanced porosity, at approx. 400 m depth, 1500 m, and 3700 m. The latter corresponds to the SE2 and is also a zone of increased permeability. Furthermore, porosity does not show a clear depth dependence. Below 4000 m the sampling is not dense enough to identify zones of enhanced porosity as clearly as for the the upper 4000 m. However, if we assume that there is also no depth dependence of the porosity below 4000 m, zones of increased porosity found at 4800 m, 6800 m, and 8000 m can also be understood as indications for fracture zones.

However, the mentioned profile (Fig. 5.7) shows slightly higher porosities than the porosities derived by Kern & Schmidt (1990). They estimate the in situ crack porosity from strain measurements on samples from the KTB-VB derived from triaxial compression experiments. Crack porosity was found to decrease from approx. 1% to 0.1% at 4000 m depth. In addition, there are hints that the total amount of stiff porosity seems to be negligible (T. Popp; pers. comm.). Especially the high porosity peaks have not been confirmed by Kern & Schmidt (1990). This might be caused by a coarser sampling of analyzed core samples. However, it is also reasonable to assume that the porosities shown in Fig. (5.7) are influenced by relaxation processes due to recovery since they were obtained from relaxed samples under room condition.

<sup>1</sup>For further information about the measurements, see <http://icdp.gfz-potsdam.de/html/ktb/ktb.htm>

### 5.4.2 Permeability of the KTB rocks

The permeability of the KTB rocks was investigated by numerous researchers using different techniques. These include the determination of matrix as well as fracture permeability on the core and wellbore scale and between the pilot and main hole. In addition to the somehow classical hydrogeological measurements, e.g., pumping tests or drill stem tests, in order to determine permeability, transmissibility, storativity and hydraulic diffusivity. In addition, the spatio-temporal distribution of induced microseismicity was also used. In the following, the different results are summarized.

The permeability  $\kappa$  is a rock property and a measure for its ability to conduct fluids. In its most general form the permeability is a 3x3 tensor. Although it is intuitive to relate permeability to porosity this relation is quite complicated and not straightforward. In fact, there are rocks with very high porosity and very low permeability, like, e.g., shales, and on the other hand rocks, e.g., some basalts, where porosity is very low and permeability is high. One reason for this complex relation is that the permeability strongly depends on the geometry and connectivity of the pore space rather than on the amount of voids.

Assuming a uniformly distributed fluid flow through a porous rock sample driven by a constant fluid pressure gradient  $\nabla h$ , the volumetric flow through the sample can be described using Darcy's law:

$$Q = k_f A \nabla h, \quad (5.1)$$

where  $Q$  is the volumetric flow rate,  $k_f$  is the hydraulic conductivity,  $A$  is the cross sectional area of the sample normal to the pressure gradient, where the fluid pressure is given in height of water column. In equation (5.1) the hydraulic conductivity depends on the conductivity of the rock and the properties of the fluid, i.e., density  $\rho_{fl}$  and dynamic viscosity  $\nu$ . Permeability and hydraulic conductivity are related by:

$$\kappa = \frac{k_f \nu}{g \rho_{fl}}, \quad (5.2)$$

where  $g$  is acceleration due to gravity. Permeability is usually given in  $m^2$  or *Darcy* (see Tab. G.1 for conversion factors).

Assume a situation where this measurement configuration samples fluid flow through two different regions with distinct permeabilities  $\kappa_F \ll \kappa_M$  over a cross sectional area  $A$ , as indicated in Fig. 5.8. In this case, the bulk permeability depends not only on  $\kappa_M$  and  $\kappa_F$  but also strongly on the area of the samples cross section, as indicated by eq. 5.1 in terms of  $k_f$ . If the high permeable layer represents a fracture and the surrounding rock mass of the sample the matrix, then  $\kappa_M$  represents the matrix permeability and  $\kappa_F$  the fracture permeability.

The fracture permeability depends on the underlying model for fluid flow through a single fracture or a set of fractures. The most common model for fluid flow through a single fracture is the cubic law. A fracture is represented by two plane plates separated by a constant aperture  $b$ . The cubic law for one-dimensional flow in x-direction reads (e.g., Brown, 1987):

$$Q = -L_y \frac{b^3}{12\nu} \frac{dP_{fl}}{dx}, \quad (5.3)$$

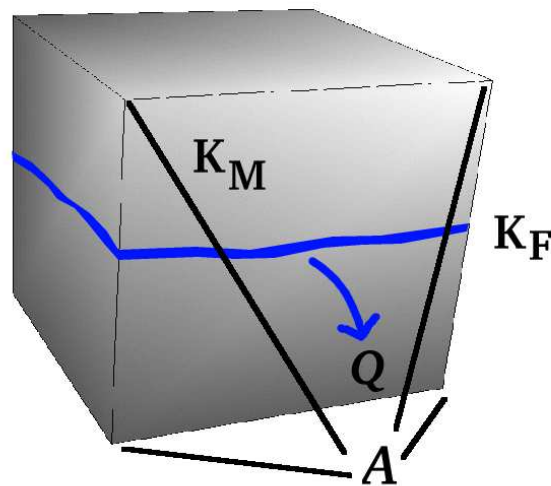


Figure 5.8: Sample with distinct permeability domains: Bulk permeability of a fractured sample results from the permeability of the fluid flow controlling fracture permeability  $\kappa_F$ , the matrix permeability  $\kappa_M$  and the considered cross sectional area  $A$ .

where  $L_y$  is the width of the fracture in the direction normal to fluid flow. A comparison of eq. (5.3) with Darcy’s law eq. (5.3) shows that the intrinsic permeability of the parallel plate fracture is

$$\kappa = \frac{b^2}{12}. \tag{5.4}$$

In order to describe the hydraulic properties of a fracture zone embedded in a host rock the fracture zone is often replaced by a set of plane parallel fractures or an hydraulically equivalent effective porous medium.

Fractured porous rocks with distinct permeability domains, i.e., high permeable fractures and a low permeable matrix are denoted as double porosity systems. The fractures are effective for fluid flow and control the bulk permeability of the rock. In contrast, the rock matrix controls the storage capacity of the rock.

A measure for the storage capacity of a porous rock is the specific storage  $S_s$ . It describes the amount of water released from or stored in a  $1 \times 1 \times 1 \text{m}^3$  cube of porous rock when the pore pressure on opposite sides of the sample changes by 1 m water height. Multiplication of  $S_s$  with the thickness of the aquifer gives the storativity  $S$ . In an unconfined aquifer the magnitude of  $S$  is usually of the order of the porosity effective for fluid flow, hence, of the order of 0.1. In contrast, in confined aquifers, where the thickness of the reservoir is constant  $S$  results mainly from the deformation of the matrix material and fluid due to pressure changes and is thus orders of magnitudes smaller than in the unconfined state.

A measure for the fertility of a reservoir is the transmissibility, or transmissivity,  $T$ . In terms of the permeability the transmissivity reads:

$$T = \kappa \cdot M \quad \text{with} \quad [T] = [m^3]. \tag{5.5}$$

In a confined reservoir,  $M$  equals the reservoir thickness. In an unconfined reservoir  $M$  is the mean thickness of the water filled volume. In hydrogeology, where the satu-

## 5.4. Rock physical properties

---

rating fluid is usually groundwater with negligible changes in viscosity and density the hydraulic conductivity  $k_f$  is used in eq. (5.5). Since  $[k_f] = [m/s]$  the transmissivity is then given in  $[m^2/s]$ .

The effect of pore pressure variations is not limited to an initiation of fluid flow alone. Variations in pore pressure lead to changes in the overall state of stress in a rock mass and thus to deformation of the rock. The time-dependent interaction of fluid flow and rock deformation is described by the theory of linear poroelasticity. For an irrotational displacement field in an infinite homogeneous and isotropic domain (with respect to the elastic and hydraulic properties) pore pressure distribution in space and time can be formulated as a diffusion equation (Shapiro *et al.*, 1997):

$$\frac{\partial P_{fl}}{\partial t} = D \cdot \nabla^2 P_{fl}. \quad (5.6)$$

Here,  $D$  is the hydraulic diffusivity and  $t$  is time. Permeability is related to  $D$  by the following equation:

$$D = \frac{\kappa}{\nu} N, \quad (5.7)$$

with

$$\begin{aligned} N &= MP_d/H \\ M &= \frac{1}{\frac{\phi}{K_{fl}} + \frac{\alpha - \phi}{K_0}} \\ P_d &= K_{dry} + \frac{4}{3} \mu_{dry} \end{aligned}$$

and  $\alpha = 1 - K_{dry}/K_0$  is the Biot coefficient. In the case of low-porosity crystalline rocks parameter  $N$  can be approximated by:

$$N = \left[ \frac{\phi}{K_{fl}} + \frac{\alpha}{K_0} \right]^{-1}. \quad (5.8)$$

The mentioned hydraulic properties  $D$ ,  $T$ ,  $S$ , and  $\kappa$  are related by (Kessels & Kück, 1995):

$$D = \frac{M\kappa}{M\nu S} = \frac{T}{\nu h S} \quad (5.9)$$

The hydraulic properties of the KTB rocks have been investigated by numerous researchers in-situ as well as in the laboratory. This includes small scale observations (in the range of cm) of fluid flow through a single fracture (Durham, 1997) and intact core samples (Morrow *et al.*, 1994) through Wire Line borehole measurements as well as pumping and injection tests in both bore holes (e.g., Kessels & Kück, 1995). Both classical hydraulic analysis approaches as well as the spatio-temporal distribution of induced microseismicity have been used to estimate the hydraulic properties of the KTB rocks.

The KTB rocks are assumed to represent a double porosity system. According to Huenges *et al.* (1997), the matrix permeability was determined in the laboratory as  $7 \times 10^{-20} \text{ m}^2$  (geometric mean) with more than a decade standard deviation. The in-situ matrix permeability is higher ranging from  $5 \times 10^{-18} \text{ m}^2$  to  $3 \times 10^{-19} \text{ m}^2$ . In general,

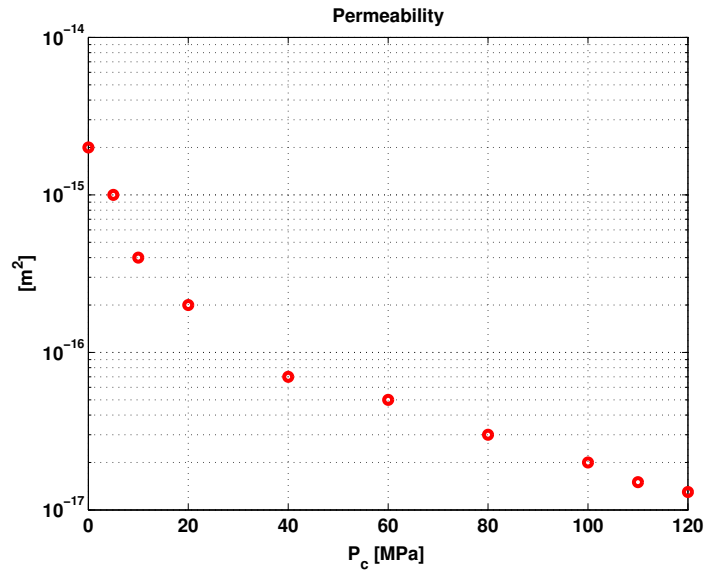


Figure 5.9: Confining pressure dependent permeability of a fracture from the KTB pilot hole (3800m), approximated from Fig. 2 in Durham (1997).

matrix permeability is anisotropic with higher values parallel ( $3 \times 10^{-19} m^2$ ) than normal ( $2 \times 10^{-20} m^2$ ) to the foliation.

Durham (1997) investigated the hydraulic properties of a single fracture on a core sample recovered from 3800 m from the KTB pilot hole. The fractured sample was subjected to isostatic confining stress (confining pressure) up to 120 MPa. Water pressure at the output end of the sample was 0.1 MPa, and never exceeded 5% of the confining pressure at the input end. Permeability decreases of the mentioned confining pressure approximately range from  $2 \times 10^{-15}$  to  $1 \times 10^{-17} m^2$ , as shown in Fig. 5.9. Fracture permeability was calculated assuming a laminar flow regime according to

$$\kappa_F = \frac{Q}{A} v \frac{dx}{dP_f}, \quad (5.10)$$

where  $P_f$  is in Pa. Under in situ conditions, assuming a hydrostatic pore pressure of 38 MPa and an effective stress ranging from 23 to 92 MPa, permeability of this sample should range from  $2 \times 10^{-16}$  to  $2 \times 10^{-17} m^2$ .

The influence of conducting fractures on the bulk permeability of a rock can be demonstrated by comparing these results with permeability estimations on intact amphibolite from 3607 m depth from the KTB pilot hole, as obtained from Morrow *et al.* (1994). The permeability of the intact rocks is 3.5 – 7 orders of magnitude below the permeability of the fractured rock, dependent on the orientation of flow with respect to the orientation of the maximum principle horizontal stress. The permeability observations of Morrow *et al.* (1994) are consistent with results from Huenges (1993) obtained on core samples from 3000 to 3800 m depth in the KTB pilot hole. There, core permeability was found to range from less than  $10^{-21}$  to  $3 \times 10^{-19} m^2$  at near zero confining pressure.

On a larger scale the permeability was investigated in situ by draw down tests. For a test interval ranging from 3800 to 4000 m depth in the pilot hole Huenges (1993) found an averaged formation permeability exceeding  $10^{-16} m^2$ . Although the formation

## 5.4. Rock physical properties

---

permeability was averaged over a 200 m interval including conducting fractures and remarkably less permeable intact regions this bulk value is higher than the (in situ) fracture permeability of the sample mentioned above. Thus, the distinct fractures in the 3800 to 4000 m interval should show a remarkable higher fracture permeability.

A build-up drill stem test at the open hole section of the main hole at 9101 m depth revealed a permeability ranging from  $5 \times 10^{-18}$  to  $1.3 \times 10^{-17} m^2$  (Huenges *et al.*, 1997). However, permeability estimations from single bore hole tests like drill stem tests may be influenced or even dominated not only by the length of the test interval but also by damage of the borehole wall due to drilling activities. This, so called skin may have significant different hydraulic properties than the undisturbed rock mass. The skin may have an extension of some cm but may also range up to a few meters or higher. In general, the permeability of the skin is higher than of the fresh rock. However, permeability may artificially be decreased by drilling mud entering the formation. It is well known from the hydrocarbon industry that drilling fluid may even seal a bore hole, especially in the case of overbalanced drilling.

Several artificial formation pressure variations in the main hole caused a hydraulic response in the pilot hole. Such pressure variations between 3000 and 6000 m depth in the main hole were observed 25 h later in the pilot hole. The minimum distance between the open hole section of the pilot hole and this interval of the main hole is 200 m. This value, hence, corresponds to the minimum length of a flow path. A pressure response in the pilot hole due to an injection experiment in the open hole section of the main hole in 9101 m indicates that a permeable fracture network exists between the bottom levels of both boreholes with a flow path of at least 5000 m length. Using the hydraulic communication data above 6000 m in the main hole Kessels & Kück (1995) found an effective fracture aperture of approx.  $6 \times 10^{-6} m$ . For the SE2 fault zone, they found a transmissivity  $T = 1.62 \times 10^{-13} m^3$ , a storativity  $S = 5.0 \times 10^{-9}$ , and a hydraulic diffusivity  $D = 0.12 m^2/s$ , assuming a fault zone width of 300 m and a viscosity of  $2.7 \times 10^{-3} Pa \cdot s$ .

Approximately 10 years after the above mentioned hydraulic tests a new research project was started at the KTB test site. One of the major experiments of this research project was a 12 month production test in the pilot hole, started in June 2002. Based on earlier derived estimations of the hydraulic parameters of the SE2 fault zone a draw down of approx. 2200 m was expected for a pumping rate of  $5 \times 10^{-4} m^3/s$  (30 l/min). However, only 1/8th of the expected draw down was reached. A first interpretation of the pumping test revealed a transmissivity of  $9.5 \times 10^{-6} m^2/s$  (Stober, 2003).

On a scale of  $km^3$  the permeability as well as the complete tensor of permeability were estimated using a quite different approach, based on the analysis of the spatio-temporal evolution of injection induced microseismicity for two injection experiments carried out at the open hole section of the main hole in 9.1 km depth in 1994 and 2000. The basic assumption of the so-called *Seismicity Based Reservoir Characterization* (SBRC) approach is that microseismicity is caused by a diffusive process of pore pressure relaxation induced by a pore pressure perturbation due to injection of fluid in a borehole.

Application of the SBRC approach to the induced microseismicity of the 1994 injection experiment revealed a scalar hydraulic diffusivity of  $0.3 m^2/s$  to  $2 m^2/s$  Shapiro *et al.* (1997). The permeability was found to be in the order of  $2.5 \times 10^{-17} m^2$  to  $10^{-16} m^2$ .

This data set was also analyzed with respect to the tensorial character of hydraulic diffusivity and permeability (Rindschwentner, 2001). The orientation of the diffusivity tensor corresponds quite well to the orientation of the SE1 fault zone as well to the orientation of the stress tensor (see Rothert *et al.*, 2003, for details).

During the 2000 injection experiment the occurrence of microseismicity was not limited to the rock volume between 8 and 9 km as in 1994. A probable leakage in the borehole casing in 5.4 km depth lead to a second injection source. This caused a pore pressure perturbation in a rock volume known to be located inbetween both prominent zones of enhanced permeability, namely, the SE1 and SE2. As shown in Fig. (5.10) this cloud is more spherical in shape than the deeper cloud and its maximum spatial extension is much smaller. This is interpreted by Rothert *et al.* (2003) as a hint for an enhanced permeability of the prominent fracture zones. Moreover, the anisotropy of permeability in the fracture zones is stronger due to preferred orientation of conducting fractures. A comparison of the spatial occurrence of microseismicity and the orientation of the global permeability tensor with amplitude images of a 3D prestack Kirchhoff migration of the ISO89-3D data set (Buske, 1999) lead Rothert *et al.* (2003) to the result that there is a mutual relation between enhanced hydraulic diffusivity and reflection seismic amplitudes at the KTB.

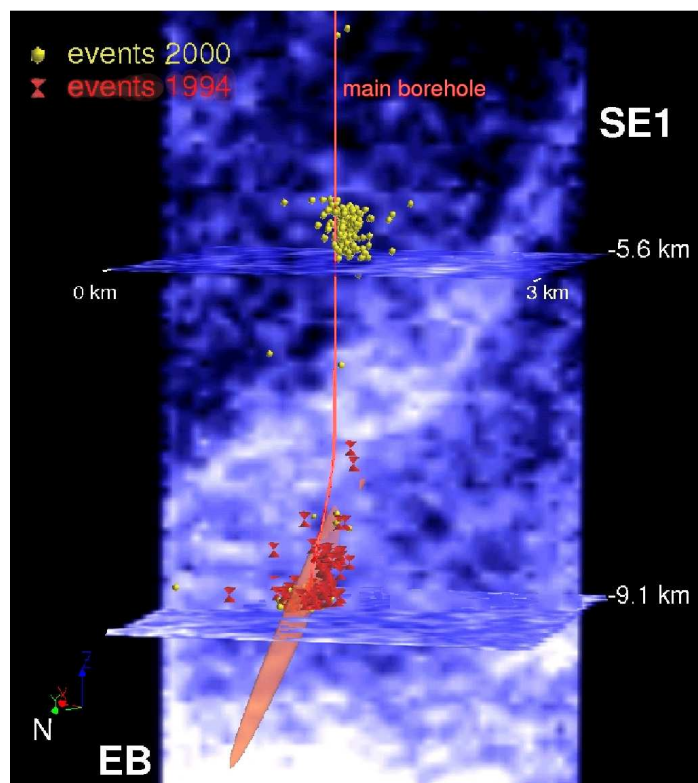


Figure 5.10: Result of 3D migration (view from NW) from Buske (1999) together with the microseismic hypocenters (events 1994=red/dark tetrahedra, events 2000=yellow/light spheres, after Baisch *et al.* (2002)) and the tensor of permeability estimated from the 1994 data set (Rindschwentner, 2001). In contrast to the 1994 events the microseismicity of the 2000 injection experiment seems to be aligned with the orientation of the seismic reflector SE1, illustrated as diffusive light line structure (Figure taken from Rothert *et al.*, 2003).

### 5.5 Reflectivity of the SE2 and induced variations

The estimation of hydraulically induced changes of the reflection response of the SE2 fault zone requires:

1. An estimation of the spatio-temporal variations of the in-situ pore pressure due to pumping or injection of fluid.
2. An estimation of the in-situ confining stress and the resulting spatio-temporal evolution of the effective stress.
3. A link between effective stress and seismic velocity changes by using laboratory experiments.
4. Calculation of acoustic in-situ fluid properties in order to calculate the stress dependent velocities of the saturated rock from the laboratory velocities of the dry rock.
5. Calculation of seismic amplitudes vs. offset (AVO-curves) for various effective stresses as resulting from pore pressure changes.

However, the mentioned approach takes only elastic deformation into account and neglects changes of elastic rock properties due to thermo-mechanical effects which might occur when cold surface water is injected into the approx. 120° C hot SE2. Moreover, it is well known from former injection experiments that even moderate fluid pressure perturbations trigger microseismic events. These events indicate non-elastic deformation of the rock volume. The effect of this rock cracking on the seismic velocities is assumed to be negligible.

It is widely accepted that the pore pressure at the KTB is hydrostatic at least down to the final depth (9101 m) of the main hole (Huenges *et al.*, 1997). The formation pressure increases with a mean gradient of 11.5 MPa/km to approx.  $103 \pm 3$  MPa, as shown in Fig. (5.6(a)). Hence, the pore pressure within the SE2, assuming a mean depth of 3900 m, is approx. 40 to 45 MPa. The spatio-temporal variation of the pore pressure within the SE2 induced by an injection experiment was estimated by W. Kessels, GGA Hannover, for a injection rate of 180 l/min. According to this approximation the pore pressure will increase in the vicinity of the borehole by approx. 4 MPa after one year of injection. With increasing distance from the bore hole the fluid pressure increase less. At a distance of 5 km the pore pressure is enhanced by 1 MPa only (Gräsle & Kessels, 2003).

During the currently finished production test a significant higher transmissivity was found in comparison to former experiments. For a pumping rate of 30 l/min the draw down was eight times smaller than expected. After increasing the discharge to 60 l/min a final draw down of 563 m was reached (Erzinger *et al.*, 2003). This corresponds to a pore pressure decrease within the bore hole of 5.63 MPa.

The complete stress tensor down to 8 km depth was estimated by Brudy *et al.* (1997). A linear approximation of the results of Brudy *et al.*, given by Ito & Zoback (2000) leads to a mean confining stress within the SE2 of approx. 120.9 MPa. This gives

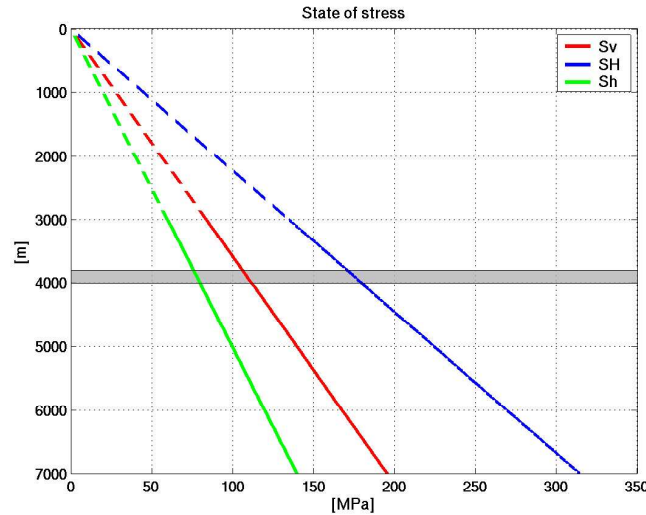


Figure 5.11: Linear approximation of confining stress at the KTB as given by Ito & Zoback (2000). The grey patch indicates the depth interval of the SE2.

for the vertical, maximum, and minimum horizontal stress  $\sigma_v = 109.2$ ,  $\sigma_H = 175.5$ , and  $\sigma_h = 78.0$  MPa, respectively, as shown in Fig. (5.11).

The effective stress for elastic moduli and, hence, seismic velocities is the difference between confining stress and pore fluid pressure, if the rock is in the Gassmann limit and/or the porosity is low. At least the latter condition is satisfied by the low-porosity KTB rocks. With a mentioned mean pore pressure of 45 MPa within the SE2 and a mean confining stress of 120.9 MPa we arrive at an initial (undisturbed) in-situ mean effective stress within the SE2 of approx. 75 to 80 MPa.

After estimations about the initial and artificially varied in-situ effective stress within the SE2 were found the link between effective stress changes and elastic velocities has to be established. It is common to establish such a stress-to-velocity transformation tool using laboratory velocity observations on core samples from the formation under consideration. Unfortunately, only one sample, KTB955C1e558 recovered from 3885 m depth from the pilot hole, can be assumed to belong to the SE2. The stress dependence of the velocities of this sample were discussed in detail in section 4.3. It was found that this sample can be assumed to be isotropic and that stiff porosity closure is negligible. As shown in Tab. 4.8 parameter D for this sample is equal to 0.019 1/MPa. Averaging parameters A and B separately for P- and S-waves gives the following velocity-to-stress transformation relations for the dry rock:

$$V_P(P_{\text{eff}}) = 6.51 - 2.08 \exp(-0.019 \cdot P_{\text{eff}}), \quad (5.11)$$

$$V_S(P_{\text{eff}}) = 3.77 - 1.09 \exp(-0.019 \cdot P_{\text{eff}}). \quad (5.12)$$

Here, velocities are in km/s and  $P_{\text{eff}}$  in MPa. Hence, an initial mean effective stress of 75 MPa gives 6.010 km/s and 3.508 km/s for P- and S-wave, respectively. Assuming, that the pore pressure variation may reach  $\pm 4$  MPa within the SE2 at least over the first Fresnel zone around the bore hole we obtain the P- and S-wave velocities for this region listed in tab. (5.2). Figure 5.12 schematically illustrates the situation.

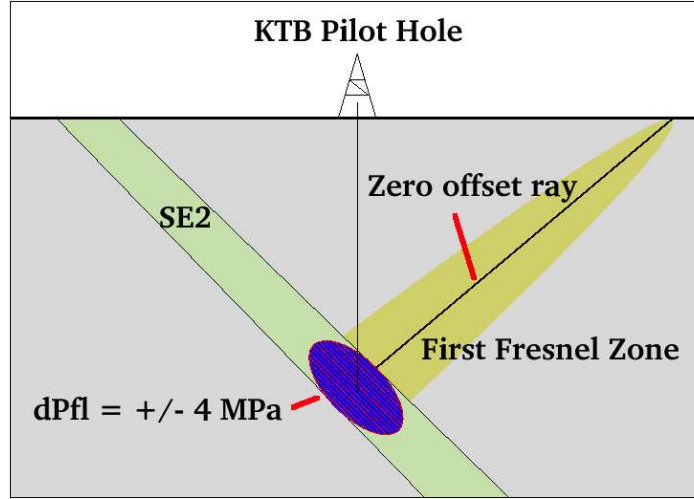


Figure 5.12: Non-scaled sketch, illustrating the model for estimation of SE2 reflectivity changes due to artificial pore pressure variation around the open hole section of the KTB pilot hole. It is assumed that pore pressure can be changed by  $\pm 4$  MPa in a volume covering at least the first Fresnel zone of the zero offset ray. Thereby, the zero offset ray is considered that is reflected from the open hole section of the pilot hole.

In order to calculate the in-situ velocities of the SE2 from the dry rock velocities mentioned before, the saturated velocities have to be calculated using Gassmann's equations (Gassmann, 1951). A velocity form of the Gassmann equations was suggested by Murphy *et al.* (1991):

$$\rho_{\text{sat}} V_{\text{Psat}}^2 = K_P + K_{\text{dry}} + \frac{4}{3}\mu, \quad (5.13)$$

$$\rho_{\text{sat}} V_{\text{Ssat}}^2 = \mu, \quad (5.14)$$

with

$$K_P = \frac{\left(1 - \frac{K_{\text{dry}}}{K_0}\right)^2}{\frac{\phi}{K_{\text{fl}}} + \frac{1-\phi}{K_0} - \frac{K_{\text{dry}}}{K_0^2}}, \quad (5.15)$$

$$\mu = \mu_{\text{dry}} = \mu_{\text{sat}}, \quad (5.16)$$

where  $\rho_{\text{sat}}$  is the density of the saturated rock,  $V_{\text{Psat}}$  and  $V_{\text{Ssat}}$  are the saturated P- and S-wave velocity, respectively,  $K_{\text{dry}}$  is the dry matrix bulk modulus,  $K_0$  the bulk modulus of the grain material,  $K_{\text{fl}}$  the bulk modulus of the saturating fluid, and  $\mu$ ,  $\mu_{\text{dry}}$ , and  $\mu_{\text{sat}}$  are the shear moduli of the rock.

In this context, the stiff porosity is a key property, since it usually builds up the major part of the bulk porosity. As shown in section (3.3) parameter A describes the P- respectively S-wave velocity of the rock under consideration with closed compliant porosity and the stiff porosity equal to  $\phi_{s0}$ . The corresponding bulk and shear moduli of such a rock with stiff porosity only can be described quite well with the upper Hashin-Shtrikman bounds as a function of  $\phi_{s0}$  and the bulk and shear modulus  $K_0$  and  $\mu_0$ , respectively, of the grain material.

If the analysis of the laboratory experiments has confirmed that the role of the stiff porosity closure in the stress dependence of the velocities is negligible, i.e., parameter

$K \approx 0$ , then the stress independent part of the stiff porosity  $\phi_{s0}$  can be approximated with the total porosity measured in the laboratory. Moreover, especially in this case the density of the rock can be assumed constant. Then, it is straightforward to solve the upper Hashin-Shtrikman bounds for  $K_0$  and  $\mu_0$  with  $\phi_{s0}$  as the independent variable. However, even if the stiff porosity changes the error resulting from the mentioned strategy should be negligible in comparison to the error introduced by using literature values for  $K_0$  and  $\mu_0$ .

The mentioned approach is quite generally applicable for most rocks. In the case of the low-porosity KTB rocks it is even more simple. Figure (4.20) shows that the velocities are approximately constant above 150-200 MPa, where stiff porosity is assumed to be completely closed. Taking additionally into account that the KTB rocks are assumed to show no stiff porosity at room conditions (T. Popp, pers. comm.) it is reasonable to assume that the velocities approach the velocities of the grain material above 200 MPa. This gives approx. 6.5 and 3.7 km/s for P- and S-waves, respectively. These velocities coincide with the mean values for AP and AS as given in equation (5.11) and (5.12). This shows that, if the rock has no significant stiff porosity, AP and AS correspond to the velocities of the grain material. With a constant density  $\rho \approx \rho_{\text{sat}} \approx \rho_{\text{dry}} = 3000 \text{ kg/m}^3$  we obtain  $K_0 = 71.99 \text{ GPa}$  and  $\mu_0 = 41.07 \text{ GPa}$ . The dry rock matrix bulk and shear moduli at 71, 75, and 79 MPa are listed in Tab. (5.2).

Table 5.2: Dry rock matrix bulk ( $K_{\text{dry}}$ ) and shear modulus ( $\mu_{\text{dry}}$ ) of the SE2 fault zone for pore pressure variations  $dP_{\text{fl}}$  at initial effective stress and due to pumping and injection tests.

	$dP_{\text{fl}}$ [MPa]	$P_{\text{eff}}$ [MPa]	$K_{\text{dry}}$ [GPa]	$\mu_{\text{dry}}$ [GPa]
Injection	+ 4.0	71	58.29	36.48
Initial	0.0	75	59.13	36.92
Pumping	- 4.0	79	59.92	37.32

If the assumption is valid that the KTB rocks consist only of crack porosity then the in-situ porosity  $\phi$  at 3900 m is approximately 0.05% (see Figure (9) in Kern *et al.*, 1991). The bulk modulus  $K_{\text{fl}}$  of the KTB pore fluid is 2.27 GPa (Huenges *et al.*, 1997).

With the mentioned values for  $K_0$ ,  $\mu_0$ ,  $K_{\text{fl}}$ , and  $\phi$  the saturated velocities at 71, 75, and 79 MPa effective stress can be calculated using equation (5.13) and (5.14). An effective stress change of  $\pm 4 \text{ MPa}$  changes the dry rock P- and S-wave wave velocities by less than 1% with respect to the initial velocities at  $P_{\text{eff}} = 75 \text{ MPa}$ . While the S-wave velocity is not affected by fluid saturation P-wave velocities increase significantly by approx. 3% despite the low porosity of the rock. However, the saturation of the rock slightly decreases its stress sensitivity. An overview over the final velocities is given in Tab. (5.3)

Figure (5.13) shows the final AVO-curves for PP (P-to-P reflection), PS, SS, and SP reflections calculated by using Zoeppritz's equations as given in Aki & Richards (1980). Therefore, the upper SE2-host rock contact is assumed to represent the interface between two half-spaces. Thus, tuning effects are neglected and the wave lengths are assumed to be significant smaller than the assumed thickness of the SE2 ( $> 300 \text{ m}$ ). The host rock velocities were set to 6.5 km/s and 3.7 km/s for P- and S-wave, respectively, as shown in Fig. (5) in Lüschen *et al.* (1996) obtained from sonic logs. A

## 5.5. Reflectivity of the SE2 and induced variations

---

Table 5.3: Dry and saturated P- and S-wave velocities of the SE2 fault zone for pore pressure variations  $dP_f$  due to pumping and injection tests. Due to the low porosity saturating effects on bulk density are neglected.

	$dP_f$	$P_{\text{eff}}$	dry rock		saturated rock	
	[MPa]	[MPa]	$V_P$ [km/s]	$V_S$ [km/s]	$V_P$ [km/s]	$V_S$ [km/s]
Injection	+ 4.0	71	5.970	3.487	6.314	3.487
Initial	0.0	75	6.010	3.508	6.330	3.508
Pumping	- 4.0	79	6.046	3.527	6.344	3.527

constant density of  $3000 \text{ kg/m}^3$  was used for both host rock and SE2.

The largest normal incidence amplitudes of approx. 0.03 and 0.01 were found for SS and PP reflection, respectively. Note that all reflectivity values are given as absolute values. In detail, for the initial effective stress of 75 MPa the normal incidence PP reflection coefficient was  $R_{PP}=0.0132$  and  $R_{SS}=0.0266$  for SS reflection. Increasing the effective stress to 79 MPa increases the seismic velocities of the SE2 and decreases the velocity contrast to the host rock. Consequently,  $R_{PP}$  and  $R_{SS}$  decrease to 0.0121 and 0.0239, respectively. Injection of fluid has the opposite effect and we obtain  $R_{PP} = 0.0145$  and  $R_{SS} = 0.0296$ . Fig. (5.13) shows the reflection coefficients for PP, PS, SP, and SS reflection up to an incidence angle of 45 degree, which is measured against the reflection interface normal. Thus, an incidence angle of zero degree corresponds to normal incidence.

With respect to the initial stress normal incidence reflection coefficients  $R_{PP}$  changes due to injection and pumping of fluid by 10% respectively -8%. In the case of  $R_{SS}$  the corresponding changes are 11% and -10%. However, the absolute magnitude of the reflection coefficients is small. In comparison, Harjes *et al.* (1997) give reflection coefficients for the SE1 between 0.1 and 0.15. While the seismic signatures of the SE1 were intensively investigated by many researches a comparably detailed analysis of the SE2 is missing. Despite this, there is an agreement that the SE2 reflectivity is considerable weaker. However, since the derived stress dependent saturated P- and S-wave velocities of approx. 6.3 and 3.5 km/s agree well with the sonic log data given by Lüschen *et al.* (1996) the obtained estimations of the initial SE2 reflectivity and its induced changes seem to be reasonable.

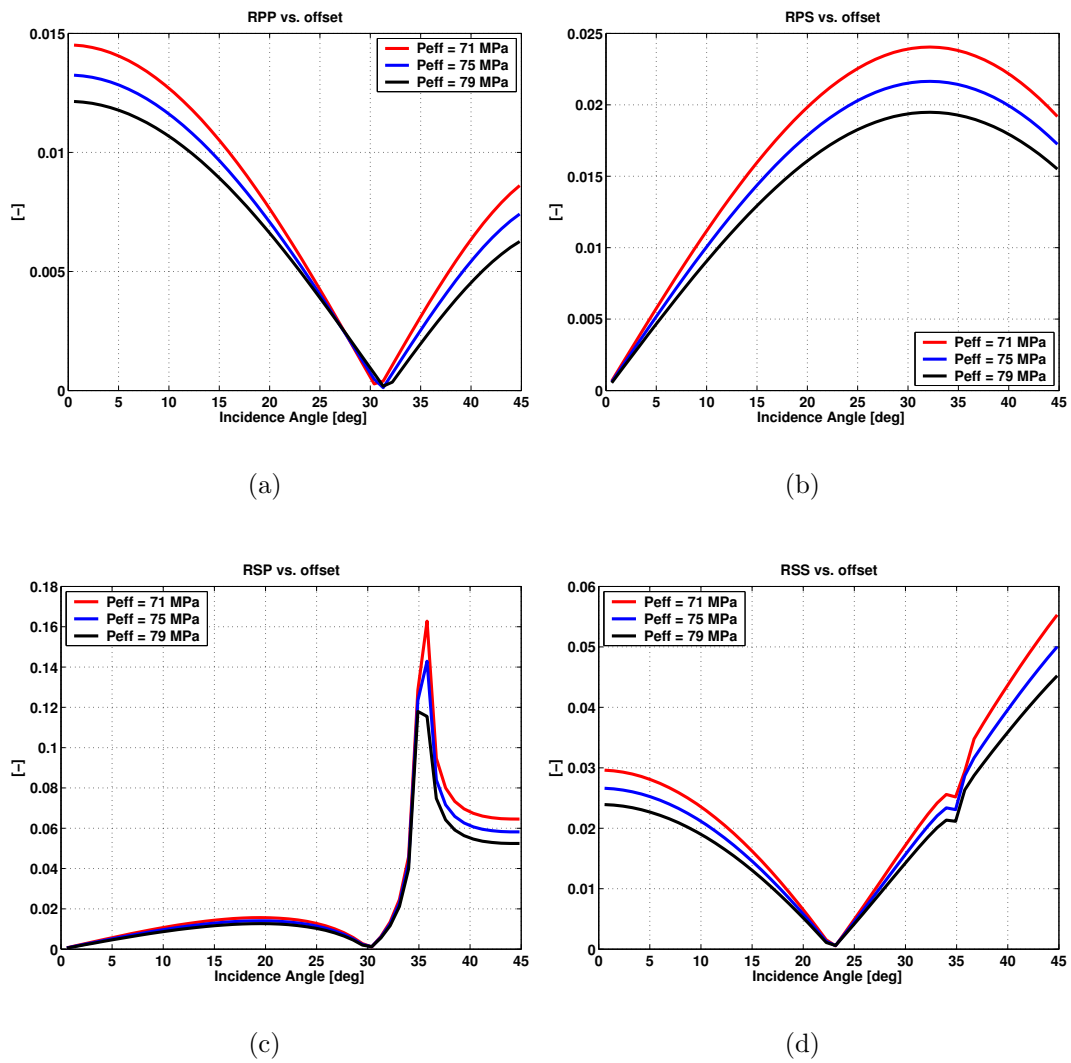


Figure 5.13: Absolute reflection coefficients of SE2-host rock interface calculated using Zoeppritz equation for 71, 75, and 79 MPa effective stress. Incidence angle is measured against the normal incidence direction.

